Red Supergiant Stars as Cosmic Abundance Probes:
II. NLTE Effects in J-band Silicon Lines

Maria Bergemann

Max-Planck-Institute for Astrophysics, Karl-Schwarzschild-Str.1, D-85741 Garching, Germany

mbergema@mpa-garching.mpg.de

Rolf-Peter Kudritzki[1,2]

Institute for Astronomy, University of Hawaii, 2680 Woodlawn Drive, Honolulu, HI 96822

kud@ifa.hawaii.edu

Matthias Würl

Max-Planck-Institute for Astrophysics, Karl-Schwarzschild-Str.1, D-85741 Garching, Germany

Matthias.Wuerl@physik.uni-muenchen.de

Bertrand Plez

Laboratoire Univers et Particules de Montpellier, Université Montpellier 2, CNRS, F-34095 Montpellier, France

bertrand.plez@univ-montp2.fr

Ben Davies

Institute of Astronomy, Univerity of Cambridge, Madingley Road, Cambridge, CB3 OHA, UK

bdavies@ast.cam.ac.uk

and

Zach Gazak

Institute for Astronomy, University of Hawaii, 2680 Woodlawn Drive, Honolulu, HI 96822

zgazak@ifa.hawaii.edu

ABSTRACT

Medium resolution J-band spectroscopy of individual red supergiant stars is a promising tool to investigate the chemical composition of the young stellar population in star forming galaxies. As a continuation of recent work on iron and titanium, detailed non-LTE calculations are presented to investigate the influence of NLTE on the formation of silicon lines in the J-band spectra of red supergiants. Substantial effects are found resulting in significantly stronger absorption lines of neutral silicon in non-LTE. As a consequence, silicon abundances determined in non-LTE are significantly smaller than in LTE with the non-LTE abundance corrections varying smoothly between -0.4 dex to -0.1 dex for effective temperatures between 3400K to 4400K. The effects are largest at low metallicity. The physical reasons behind the non-LTE effects and the consequences for extragalactic J-band abundance studies are discussed.

Subject headings: galaxies: abundances — line: formation — radiative transfer — stars: abundances — stars: late-type — supergiants

1. Introduction

With their enormous luminosities of 10^5 to $\sim 10^6$ L/L$_\odot$ (Humphreys & Davidson 1979) emitted at infrared wavelengths red supergiant stars (RSGs) are ideal probes of extragalactic cosmic abundances. The J-band spectra of RSGs are dominated by strong and isolated atomic lines of iron, titanium, silicon and magnesium, while the molecular lines of OH, H_2O, CN, and CO are weak. In consequence, medium resolution spectroscopy in this spectral range is sufficient to derive stellar parameters and chemical abundances of RSGs from these atomic lines. This has been demonstrated recently by Davies et al. (2010) (hereinafter DKF10), who introduced a novel technique using MARCS model atmosphere spectra (Gustafsson et al. 2008) to determine metallicities with an accuracy of ~ 0.15 dex per individual star. With existing telescopes and forthcoming new efficient MOS spectrographs such as MOSFIRE at Keck and KMOS at the VLT the technique can be applied to an investigation of metallicities of galaxies up to 10 Mpc distance. Even more exciting are the perspectives of the use of future adaptive optics (AO) MOS IR spectrographs at the next generation of extremely large telescopes. Evans et al. (2011) estimate that with instruments like EAGLE at the E-ELT and IRMS at the TMT it would be possible to measure abundances of α- and iron-group elements of individual RSGs out to the enormous distance of 70 Mpc.

This is a substantial volume of the local universe containing entire groups and clusters of galaxies, for which the formation and evolution could be studied through the determination of accurate abundances from individual stars. So far, most of our information about the metal content of star forming galaxies is obtained from a simplified analysis of the strongest H II region emission lines. As discussed by Kudritzki et al. (2008, 2012) and Bresolin et al. (2009) these "strong-line methods" are subject to large systematic uncertainties, which are poorly understood. In consequence, alternative methods using stars such as blue supergiants (Kudritzki et al. 2012) or RSGs are highly desirable.

We have, therefore, started to investigate the DKF10 J-band method and its possible limitations

[1]Max-Planck-Institute for Astrophysics, Karl-Schwarzschild-Str.1, D-85741 Garching, Germany

[2]University Observatory Munich, Scheinerstr. 1, D-81679 Munich, Germany

and systematic uncertainties in more detail. Since the MARCS model atmosphere spectra are calculated in local thermodynamic equilibrium (LTE), an obvious part of such an investigation is the assessment of the influence of departures from LTE, which might be important because of the extremely low gravities and hence low densities encountered in the atmospheres of RSGs. In a first step, we have carried out non-LTE (NLTE) line formation calculations in RSG atmospheres for iron and titanium and have discussed the consequences of NLTE-effects for the J-band analysis (Bergemann et al. 2012, hereafter Paper I). It was found that NLTE-effects are small for J-band iron lines, but significant for titanium. Now we extend this work and present detailed NLTE calculations for silicon. There are four strong sub-ordinate Si I lines observed in J-band spectra of RSGs, which provide crucial abundance information. We investigate the influence of NLTE effects on the formation of these lines.

The paper is structured as follows. In sections 2 we describe the model atmospheres and the details of the line formation calculations. Section 3 presents the results: departure coefficients, line profiles and equivalent widths in LTE and non-LTE and non-LTE abundance corrections for chemical abundance studies. Section 4 discusses the consequences for the new J-band diagnostic technique and aspects of future work.

2. Model Atmospheres and non-LTE Line Formation

As in Paper I we use MARCS model atmospheres (Gustafsson et al. 2008) for the underlying atmospheric structure and the DETAIL NLTE code (Butler & Giddings 1985) for the calculation of NLTE occupation numbers. Line profiles and NLTE abundance corrections are computed with the separate code SIU (Reetz 1999) using the level departure coefficients from DETAIL. SIU and DETAIL share the same physics and line lists. For all details such as model structure and geometry, background opacities, solar abundance mixture, etc. we refer the reader to Paper I.

To assess the importance of NLTE effects for the J-band Si I lines we use a small grid of models computed assuming a stellar mass of 15 $M_\odot$ with five effective temperatures (T$_{\mathrm{eff}}$ = 3400, 3800, 4000, 4200, 4400K), three gravities (log$\,g$ = 1.0, 0.0, −0.5 (cgs)), three metallicities ([Z]$\equiv$ log Z/Z$_\odot$ = −0.5, 0.0, +0.5).

The micro-turbulence is fixed to $\xi_t = 2$ km/s. This grid covers the range of atmospheric parameters expected for RSG's (see DKF10 and Paper I).

2.1. Model atom

Our model atom consists of the first three ionization stages of silicon. It has 289 levels of Si I (mostly singlet and triplet terms and one quintet term), 50 levels of Si II (duplet and quartet terms). Si III is represented by its ground state only because of the low effective temperatures of RSGs, for which Si I is the dominating ionization stage in the atmospheric layers where the IR lines investigated in this study form. Fine structure splitting is taken into account for all Si I levels with excitation energies smaller than 7.45 eV and all Si II levels with excitation energies smaller than 6.20 eV. Most of the information on energy levels was drawn form the NIST database (Kramida et al. 2012)[1]. Also, 147 theoretically-predicted Si I levels were included from the Kurucz database[2]. Atomic completeness at energies close to first ionization threshold is important for statistical equilibrium of the neutral atom.

The radiative bound-bound transitions between energy levels of Si I were extracted from the Kurucz database, while the Si II data have been taken from the NIST database. There is no need for a more refined model of Si II since the ion is un-affected by non-LTE for FGKM stars, which is also confirmed by our test calculations. In fact, on these grounds the whole Si II stage could be excluded completely. Only transitions between $0.1 \mu m$ and $30 \mu m$ with $\log gf$-values greater than -8 were included. In total, the model atom contains 2956 allowed transitions, 2826 for Si I and 130 for Si II respectively. Fig. 1 shows the complete atomic model.

While Fig. 1 gives an impression about the total effort made in calculating NLTE effects for the silicon atom, it is not well suited to discuss the conditions leading to the formation of the IR J-band Si I lines. For this purpose, we provide Fig. 2, which shows only transitions from and to the upper and lower levels of these lines. Fig. 3 zooms into this figure and displays the corresponding fine structure splitting. The detailed information about the lines is given in Table 1.

Photoionization cross-sections calculated in the close coupling approximation using the R-matrix method were taken from the TOPbase database (Cunto et al. 1993) and are limited to a minimum of photon wavelengths of 1000Å. About 20 % of very high levels with excitation energy above 6 eV were missing in this database and for those the hydrogenic approximation was adopted.

Electron collisions for excitation and ionization were calculated using the approximations by van Regemorter (1962) and Seaton (1962), respectively, as also given by Cox (2000, Sections 3.6.1, 3.6.2). Bound-bound and bound-free collision cross-sections due to collisions with H I atoms were calculated according to the generalized formula given by Lambert (1993, A10).

2.2. Test calculations for the Sun

As a test of our approach to model the formation of silicon lines we have calculated Si I and Si II lines for the Sun and determined their non-LTE silicon abundances. For the optical lines, the gf and C_6 values were taken from Shi et al. (2008), and the microturbulence set to 1 km/s. The result is $\log A_{Si} = 7.56 \pm 0.05$ in a very good agreement with the non-LTE analysis by Shi et al. (2008) and Wedemeyer (2001). The NLTE abundance corrections for the lines in common are also fully consistent with the latter investigations: the NLTE effects in the optical Si I transitions are minor, typically within -0.01 ± 0.01 dex, but become increasingly important for the IR lines, reaching -0.1 dex.

A comparison with the observed silicon IR J-band in the solar KPNO flux spectrum is given in Fig. 4. The gf-values are that recommended by the VALD2 database, i.e., Kurucz (2007). The non-LTE calculations agree well with the observations in the line cores as well as in the wings. This confirms that the atomic data used for the lines (gf-values, radiative and collisional broadening) are reliable. The LTE line profiles are substantially weaker showing that LTE is a poor approximation for the solar IR Si I lines and leading to 0.05 to 0.1 dex over-estimated abundances.

Based on the solar analysis, we do not find any need for an arbitrary scaling of the cross-sections in the NLTE calculations, contrary to Shi et al. (2008). They obtain a somewhat better fit for the 12031 Å Si I line adopting a lower efficiency of H I inelastic collisions. There could be several reasons for that. First, they used a different source of gf-values (Hartree-Fock data from http://nlte.nist.gov/MCHF/). Second, they could have assumed a different value of micro- and macroturbu-
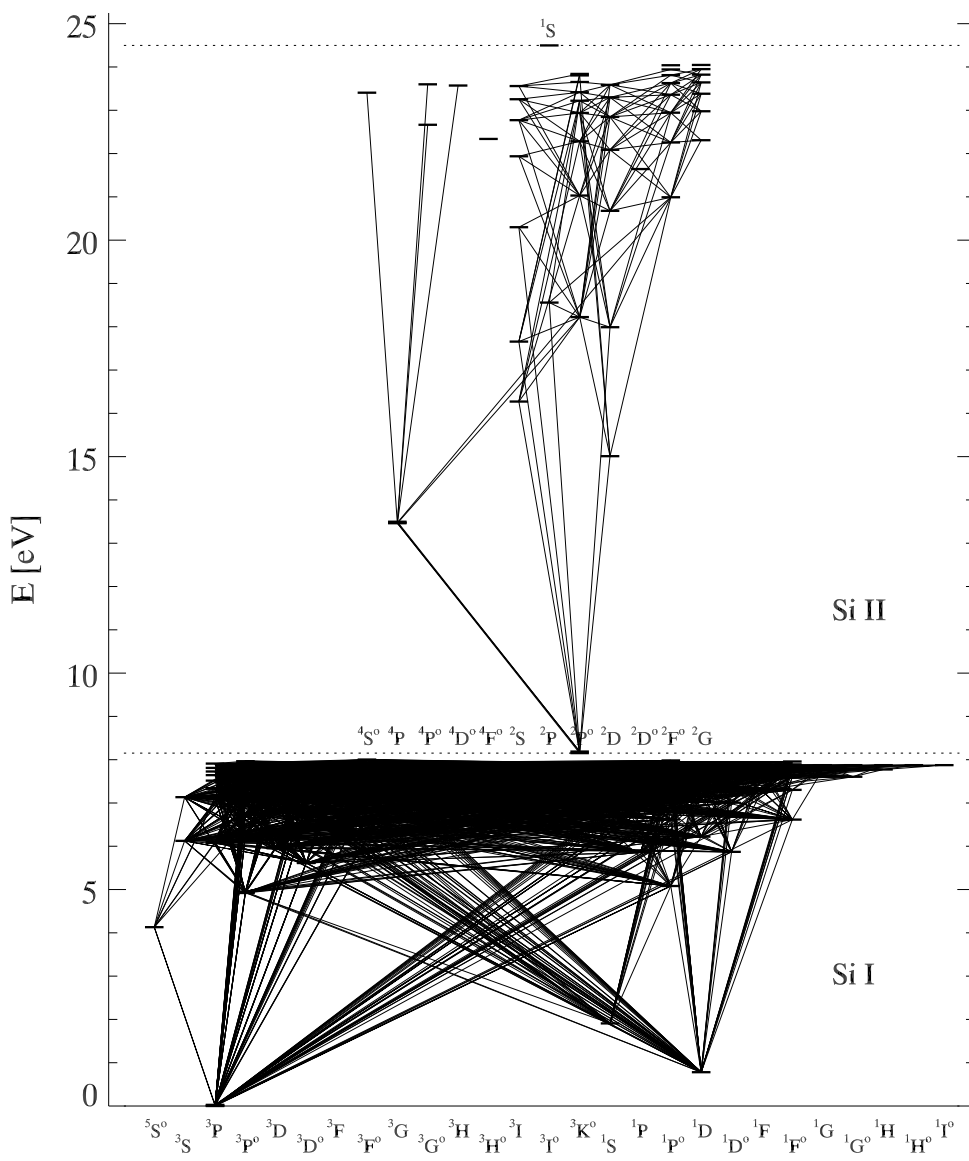

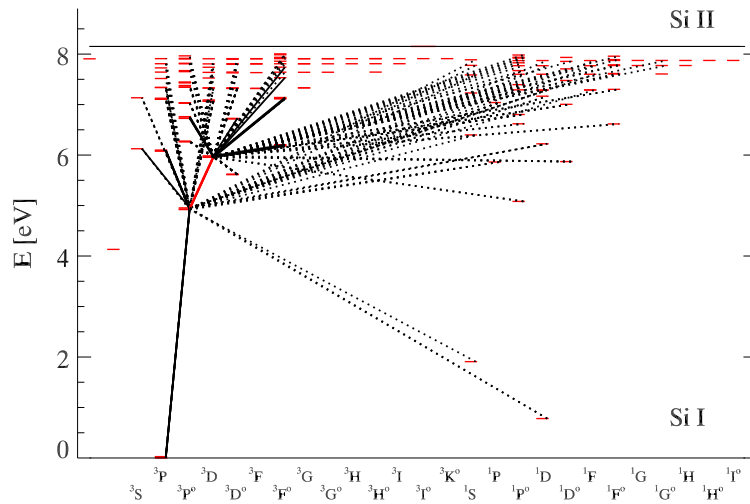Fig. 1.— The complete silicon atomic model.

Fig. 2.— The silicon NLTE atomic model showing only transitions to and from the levels leading to the J-band IR transitions. Strong transition with $\log gf$-values larger than -1.0 are solid, weaker transitions are dotted. The IR transitions are highlighted in red.
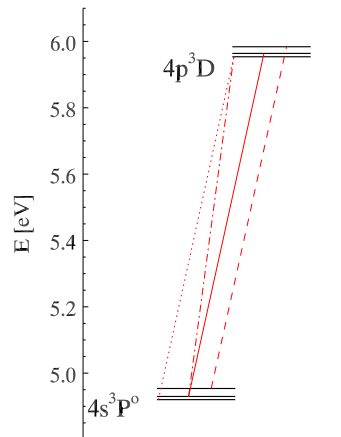

Fig. 3.— Fine structure splitting of the Si I IR J-band lines.

lence. Unfortunately, Shi et al. (2008) do not provide ξ_t and V_{mac} in the paper for us to make a detailed comparison.
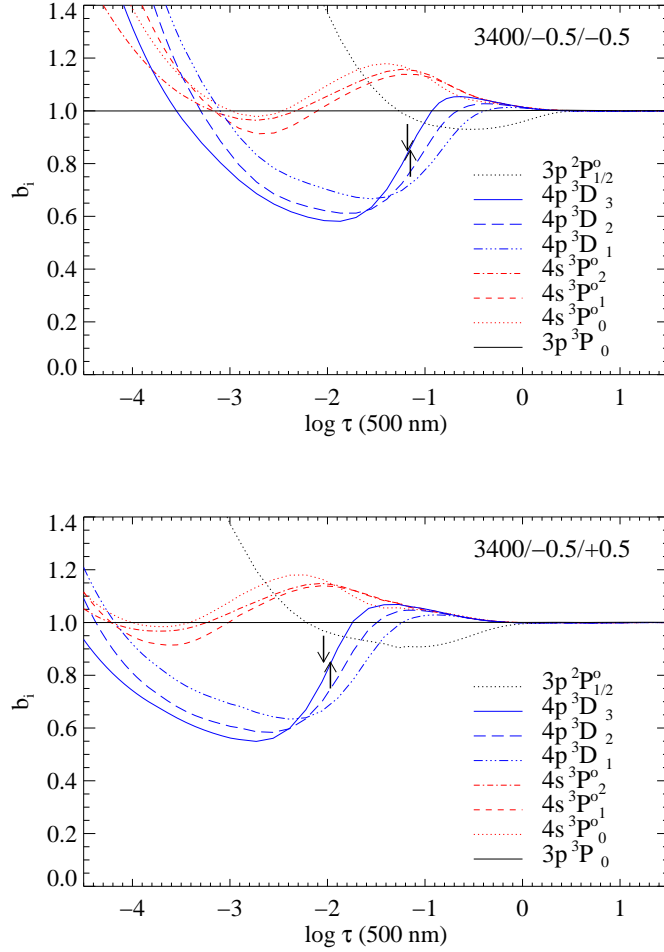
Fig. 5.— The NLTE departure coefficients of Si I for RSG models with $T_{\text{eff}} = 3400$K, log g = −0.5 and [Z] = −0.5 (top) and 0.5 (bottom) and as a function of optical depth. Black solid: Si I ground state, black dotted: Si II ground state. Red: lower fine structure levels of J-band IR transitions. Blue: upper fine structure levels of IR-transitions. The LTE and NLTE line core optical depths $\log \tau(12031\,\text{Å},\,\text{Si I}) = 0$ are also indicated by the upward and downward directed arrows, respectively.

3. Results

Given the very complex atomic structure with thousands of radiative and collisional processes contributing to the net population or de-population of levels a comprehensive quantitative discussion of the NLTE effects is complicated. For simplicity, we focus on the Si I levels and transitions related to the J-band analysis of RSG stars and on the ground states of Si I and Si II . Fig. 5 and 6 show the departure coefficients b_i of the

corresponding levels defined as

$$b_i = n_i^{\text{NLTE}} / n_i^{\text{LTE}} \qquad (1)$$

where n_i^{NLTE} and n_i^{LTE} are NLTE and LTE atomic level populations [cm^{-3}], respectively.

The discussion of the NLTE effects in the lower 4s ^{3}P and upper 4p ^{3}D levels of the J-band IR transitions is straightforward. The only channel for an allowed downward radiative decay of the lower state is
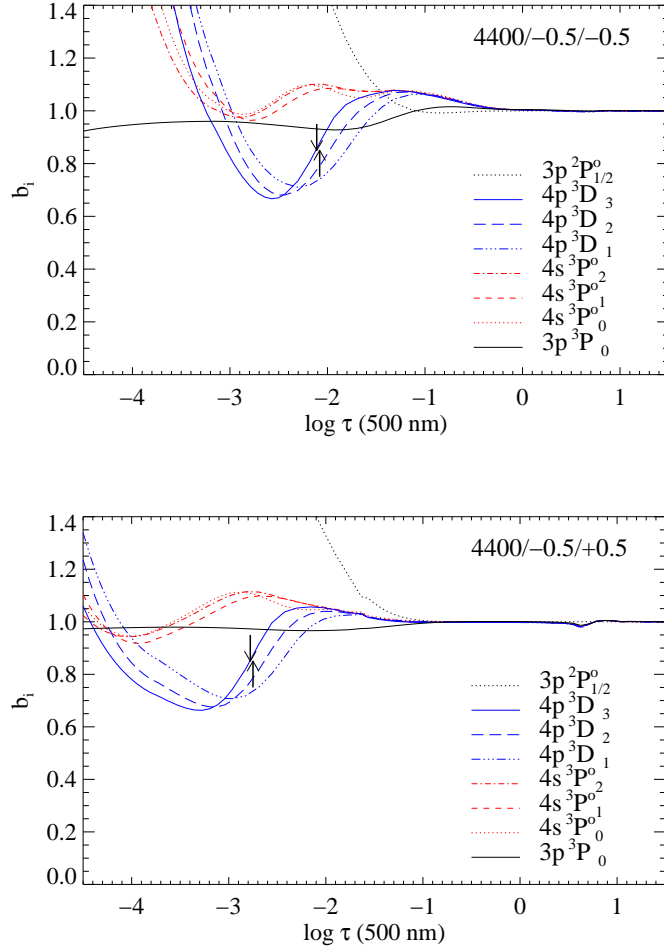
6

Fig. 6.— Same as Fig. 5 but for T_{eff} = 4400K.

towards the Si I ground state through a resonance transition. These resonance transitions (at 2506 Å, 2514 Å, 2515 Å, respectively) are optically thick throughout the formation depths of the J-band lines. This means that downward electron cascades from higher levels effectively stop at 4s ^{3}P, which causes a slight overpopulation ($b_i > 1$) of these levels. At the same time the upper levels 4p ^{3}D are depopulated ($b_j < 1$)[3] by spontaneous transitions. In consequence, the line source function S_{ij} is smaller than the local Planck function $B_\nu(T_e)$ because of $S_{ij}/B_\nu(T_e) \sim b_j/b_i < 1$. This weakening of the line source function (the ratio of line emission to absorpion coefficient) together with a slight strengthening of the line absorption coefficient through $b_i > 1$, leads to Si I absorption lines which are stronger in NLTE than in LTE (Fig. 7 and 8). Fig. 9 shows the NLTE and LTE line profiles in comparison with the observations of the Per OB1 RSG HD 14270 obtained with the IRCS spectrograph at SUBARU telescope (R $\sim 20\,000$). The fit profiles have been calculated with $T_{eff} = 3800$, $\log g = 1.0$, [Z] = 0.0, $\xi_t = 5$ km/s. The NLTE effects are clearly distinguishable when compared to the observed spectrum. Therefore, one of our next steps will be to test the new NLTE models on

---

[3]Hereafter, i and j subscripts stand for the lower and upper level, respectively, and b_i, b_j are the corresponding departure coefficients, i.e., the ratio of NLTE to LTE occupation numbers.
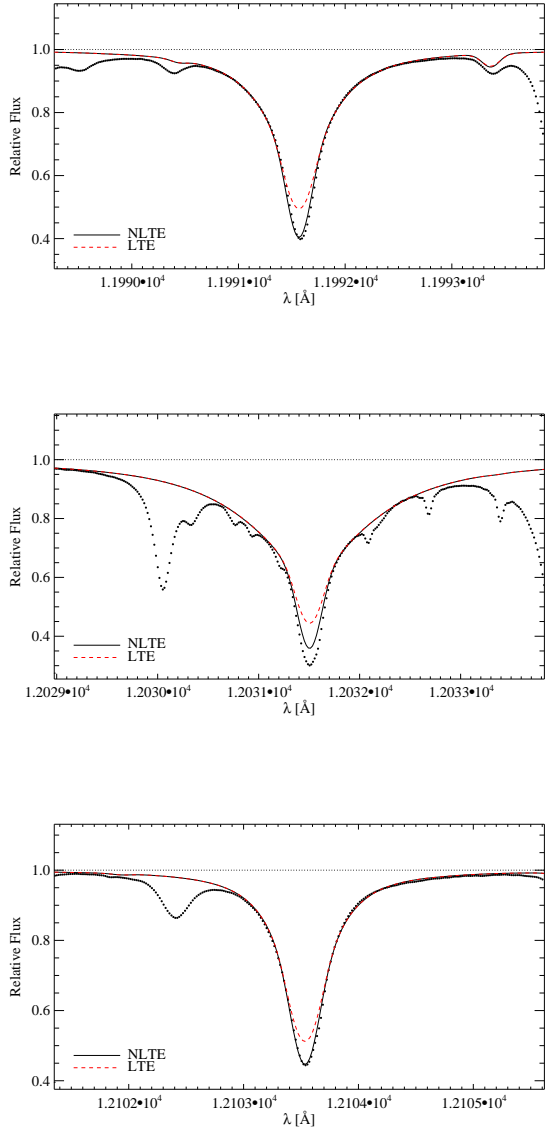
Fig. 4.— J-band observations of Si I lines in the spectrum of the Sun compared with LTE (red dashed) and non-LTE (black solid) calculations.

a large sample of high-resolution spectra of Galactic RSG's.

From inspection of Fig. 5 we see that for T_{eff} = 3400K the departure coefficients assume values of $b_i \sim 1.15$ and $b_j \sim 0.6$ at the depths of the formation

of the line cores. These values are independent of the silicon abundance (or metallicity [Z]). The only effect of higher abundance is that the line cores form further out in the atmosphere, while the extreme values of the departure coefficients remain the same. In consequence, following the Eddington-Barbier relationship that the emergent flux is roughly given by the source function at optical depth $2/3$ the relation between the NLTE and LTE emergent flux at the line center is $H_0^{NLTE} \sim \frac{b_j}{b_i} H_0^{LTE} \sim 0.5 H_0^{LTE}$. This is confirmed by the actual calculations of line profiles at both metallicities (Fig. 7).

At T_{eff} = 4400K the NLTE effects are smaller and we obtain $b_i \sim 1.1$ and $b_j \sim 0.7$, and $H_0^{NLTE} \sim 0.64 H_0^{LTE}$ (Fig 6 and 8). The reason is that at higher temperature the rate of electron collisions populating or depopulating the higher and lower levels increases, whereas the depopulation of the higher levels through spontaneous emission is temperature independent.

The increase of the absorption strengths of the Si I J-band lines in NLTE has consequences for the determination of element abundances. The importance of this effect can be assessed by introducing NLTE abundance corrections Δ, where:

$$\Delta = \log A(Si)_{NLTE} - \log A(Si)_{LTE} \qquad (2)$$

is the the logarithmic correction, which has to be applied to an LTE silicon abundance determination of a specific line, $\log A$, to obtain the correct value corresponding to the use of NLTE line formation. We calculate these corrections at each point of our model grid for each line by matching the NLTE equivalent width through varying the Si abundance in the LTE calculations. Note that from the definition of Δ a NLTE abundance correction is negative, when for the same element abundance the NLTE line equivalent width is larger than the LTE one, because it requires a higher LTE abundance to fit the NLTE equivalent width. Figs. 10 and 11 show the NLTE abundance corrections calculated in this way for the two values of microturbulence bracketing the values found in RSG's (Davies et al. 2010). It can be seen that the difference between them is small, similar to our results for the Fe I and Ti I J-band lines (Bergemann et al. 2012). Therefore, the data are given in Table 2 for $\xi = 2$ km/s only.

The NLTE abundance corrections are substantial with large negative values between -0.4 to -0.1 dex. The corrections are strongest at low silicon abundance (or low metallicity [Z]). While as discussed above

8

changes between LTE and NLTE central line intensity and, thus, also changes in the absolute value of equivalent widths W_λ are roughly independent of abundance (see Table 3), relative changes of W_λ are significantly larger at low abundance, where the lines are weaker. This in turn leads to significantly larger NLTE abundance corrections. As also discussed above NLTE effects are weaker at higher effective temperature, which decreases the NLTE abundance corrections.

In NLTE studies, it is common to investigate the dependence of NLTE effects on inelastic collision rates with H I. The prescriptions we adopted for the Si I model atom are described in Sec. 2.1 and, to the best of our knowledge, there are presently no better alternatives. While it is unlikely that we underestimate the collision strengths (Barklem et al. 2011), there is a certain degree of uncertainty with respect to their lower limit. We thus performed a series of test calculations decreasing uniformly the H I cross-sections for all Si I levels by a factor of two and ten, $S_H = 0.5, 0.1$. This scaling has a very regular effect on the NLTE corrections for different J-band Si I lines. In particular, for $S_H = 0.1$, the NLTE abundance corrections (Table 2) change by ~ -0.07 to -0.15 dex at any T_{eff} and [Z]. Clearly, more accurate estimates of the collision rates are desirable and, once available, will significantly improve the accuracy of the calculations.

4. J-band medium resolution spectral analysis and future work

In order to assess the influence of the NLTE effects on the J-band medium resolution metallicity studies, we extend the experiment already carried out in Paper I. We calculate complete synthetic J-band spectra with MARCS model atmospheres and LTE opacities for all spectral lines except the lines of Si I, Fe I, and Ti I, for which we used our NLTE calculations. We then use these synthetic spectra calculated for different metallicity with a fixed log g and effective temperature (and with added Gaussian noise corresponding to S/N of 200) as input for the DKF10 χ^2 analysis using MARCS model spectra calculated completely in LTE. From the metallicities recovered in this way we can estimate the possible systematic errors when relying on a complete LTE fit of RSG J-band spectra.

The results of this experiment are summarized in Fig.12 and reflect the qualitative behaviour of Fig. 10 except that the total metallicity corrections are smaller than the individual silicon abundance corrections. This
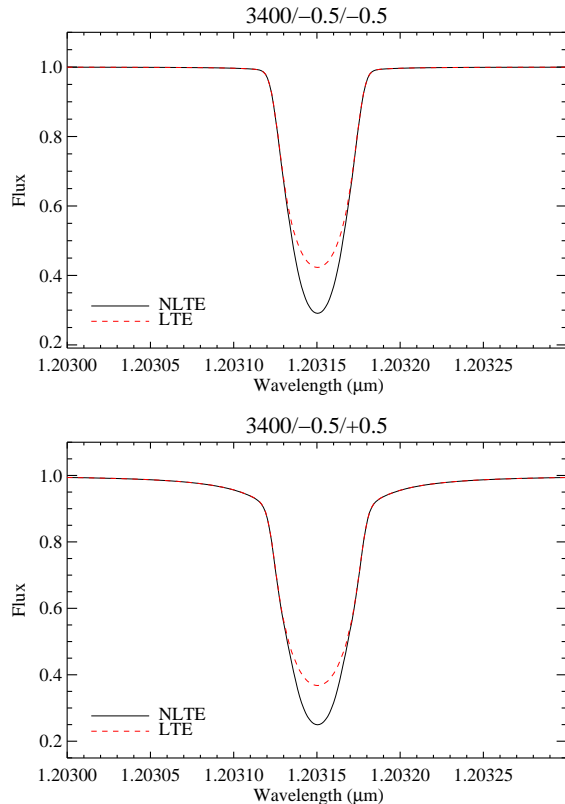
Fig. 7.— The NLTE (black, solid) and LTE (red, dashed) profiles of the Si I line at 12031 Å computed for T_{eff} = 3400K, log g = -0.5 and with [Z] = -0.5 (top) and 0.5 (bottom). The microturbulence is $\xi_t = 2$ km/s.

is caused by the fact that the metallicity determination with the DKF10 method is dominated by the numerous Fe I lines, which are relatively well represented by the LTE approximation (see Paper I). However, at lower effective temperature we still find corrections between -0.15 to -0.25 dex equal or even larger than the 0.15 dex uncertainties encountered with the DKF10 technique. In consequence, the inclusion of NLTE effects in the Si I Ti I and Fe I lines will definitely improve the accuracy of future extragalactic RSG J-band abundance studies.

4400/−0.5/−0.5

4400/−0.5/+0.5
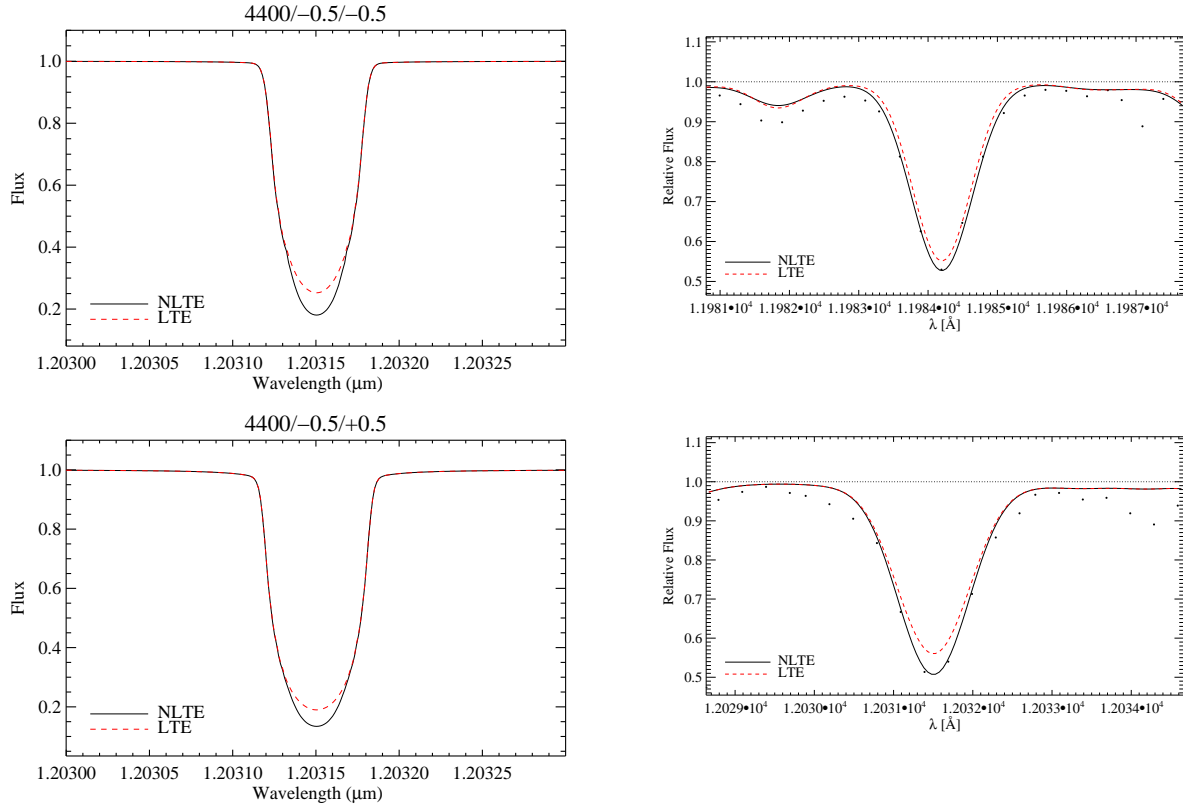
Fig. 8.— Same as Fig. 7 but T_{eff} = 4400K.

and the University Observatory Munich, where part of this work was carried out.

REFERENCES

Allen, C. W. 1973, London: University of London, Athlone Press, —c1973, 3rd ed.,

Allende Prieto, C., Lambert, D. L., & Asplund, M. 2001, ApJ, 556, L63

Barklem, P. S., Belyaev, A. K., Guitou, M., et al. 2011, A&A, 530, A94

Bergemann, M., Kudritzki, R.- P., Plez, B., et al. 2012, ApJ, 751, 156

Bresolin, F., Gieren, W., Kudritzki, R.-P., et al. 2009, ApJ, 700, 309

Brott, A. M., Hauschildt, P. H., "A PHOENIX Model Atsmophere Grid for GAIA", ESAsp, 567, 565
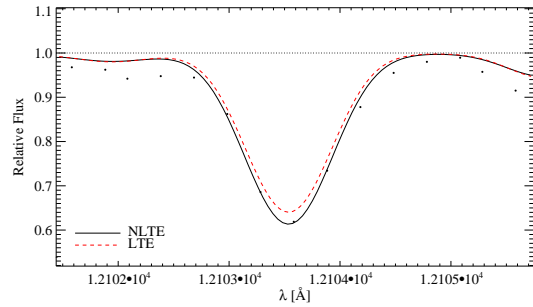
Fig. 9.— Subaru/IRCS high resolution observations (black dots) J-band observations of Si I lines in the spectrum of the Per OB1 RSG HD 14270 (top: 11984 Å middle: 12031 Å bottom: 12103 Å) compared with a LTE (red, dashed) and a NLTE (black, solid) fit. The fit profiles have been calculated with T_{eff} = 3800, $\log g$ = 1.0, [Z] = 0.0, ξ_t = 5 km/s.

Butler, K., Giddings, J. 1985, Newsletter on Analysis of Astronomical Spectra No. 9, University College

London

Chiavassa, A., Freytag, B., Masseron, T., & Plez, B. 2011, A&A, 535, A22

Cox, A. N. 2000, Allen's Astrophysical Quantities

Cunto W., Mendoza C., Ochsenbein F., Zeippen C.J., 1993, A&A 275, L5

Davies, B., Kudritzki, R. P., & Figer, D. F. 2010, MN-RAS, 407, 1203 (b)

Evans, C. J., Davies, B., Kudritzki, R. P., et al. 2011, A&A, 527, 50

Grevesse, N., Asplund, M,& Sauval, A. J. 2007, Space Sci. Rev., 130, 105

Gustafsson, B., Edvardsson, B., Eriksson, K., Jorgensen, U. G., Nordlund, A, & Plez, B. 2008, A&A, 486, 951

Kramida, A., Ralchenko, Yu., Reader, J., and NIST ASD Team (2012). NIST Atomic Spectra Database (ver. 5.0), [Online]. Available: http://physics.nist.gov/asd [2012, August 6]. National Institute of Standards and Technology, Gaithersburg, MD

Humphreys, R. M., & Davidson, K. 1979, ApJ, 232, 409

Kudritzki, R.-P., Urbaneja, M. A., Bresolin, F., et al. 2008, ApJ, 681, 269

Kudritzki, R.-P., Urbaneja, M. A., Gazak, Z., et al. 2012, ApJ, 747, 15

Kurucz, R.-L. 2007, "Robert L. Kurucz on-line database of observed and predicted atomic transitions", kurucz.harvard.edu

Lambert, D. L. 1993, Physica Scripta Volume T, 47, 186

Plez, B. 1998, A&A, 337, 495

Plez, B. 2010, ASPC 425, 124

van Regemorter, H. 1962, ApJ, 136, 906

Reetz, J. 1999, PhD thesis, LMU München

Seaton, M. J. 1962, Atomic and Molecular Processes, 375

Shi, J. R., Gehren, T., Butler, K., Mashonkina, L. I., Zhao, G. 2008, A&A, 486, 303

Steenbock, W., & Holweger, H. 1984, A&A, 130, 319

Wedemeyer, S. 2001, A&A, 373, 998
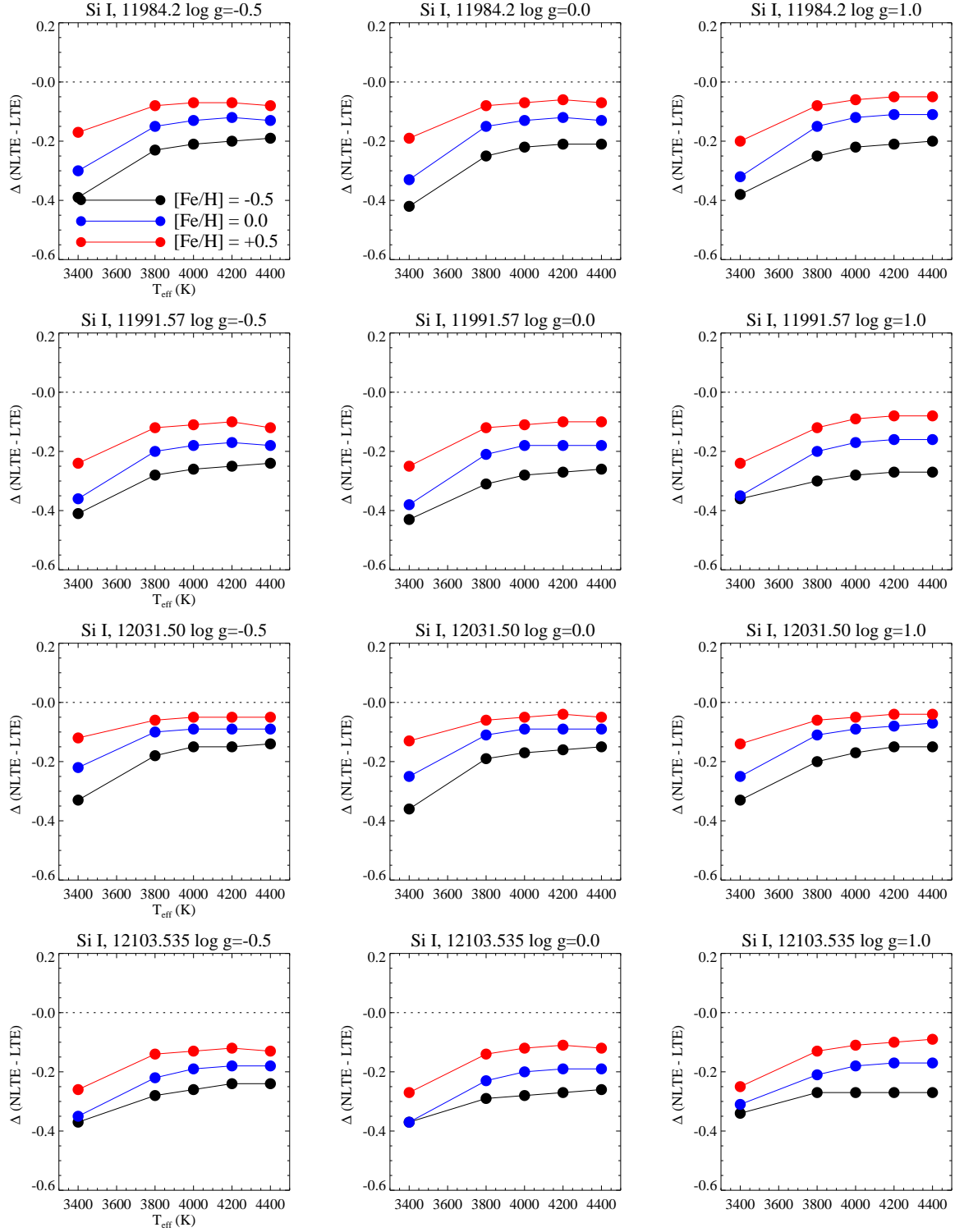
Fig. 10.— NLTE abundance corrections as a function of effective temperature for microturbulence $\xi = 2$ km/s for Si I 11984 Å (top), 11991 Å (2nd row), 12031 Å (3rd row) and 12103 Å (bottom). Left column: log g = -0.5, middle column: log g = 0.0, right column: log g = 1.0. Black solid: [Z] = -0.5, blue solid: [Z] = 0.0, red solid: [Z] = +0.5.
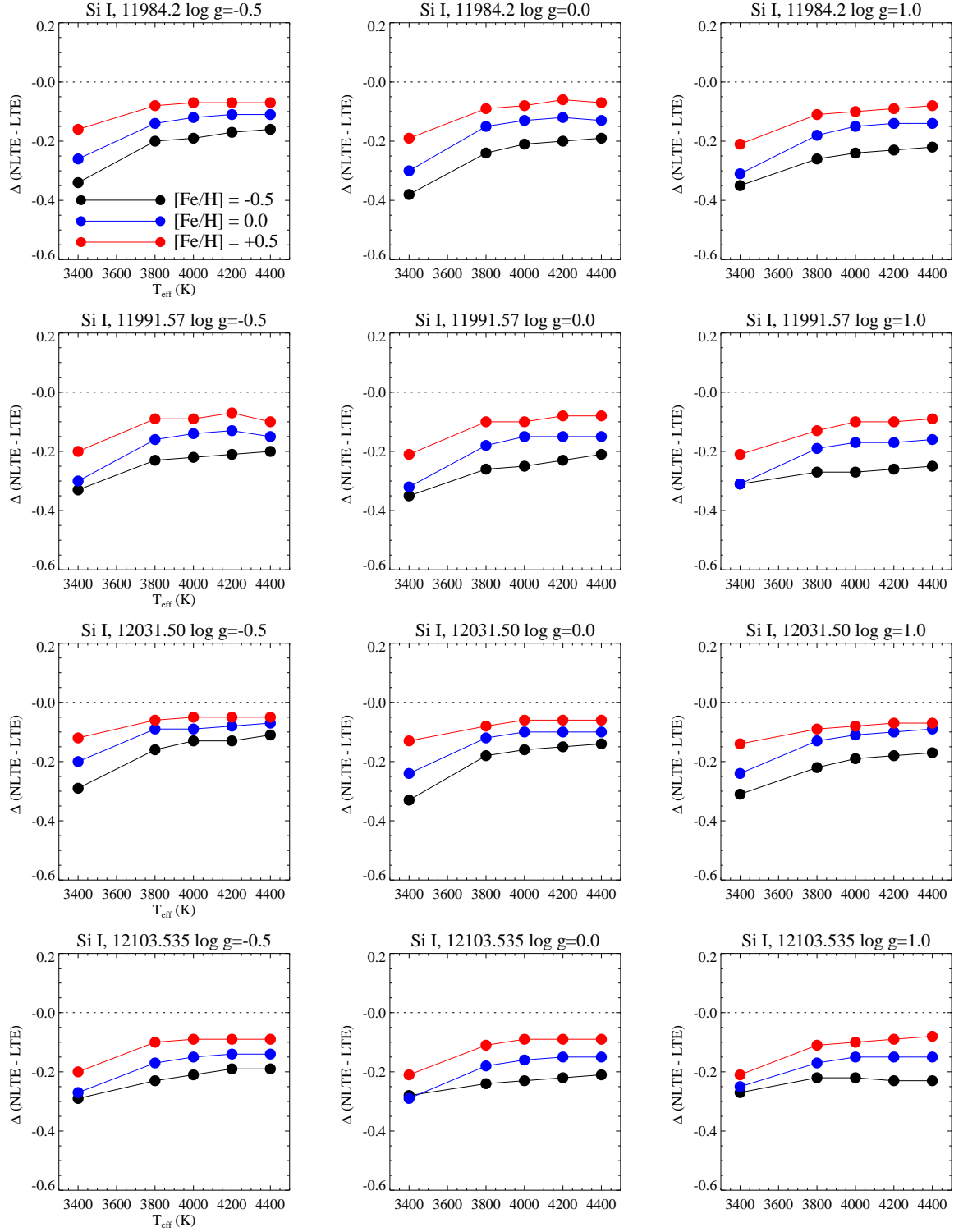
Fig. 11.— NLTE abundance corrections as a function of effective temperature for microturbulence $\xi = 5$ km/s for Si I 11984 Å (top), 11991 Å (2nd row), 12031 Å (3rd row) and 12103 Å (bottom). Left column: log g = -0.5, middle column: log g = 0.0, right column: log g = 1.0. Black solid: [Z] = -0.5, blue solid: [Z] = 0.0, red solid: [Z] = +0.5.
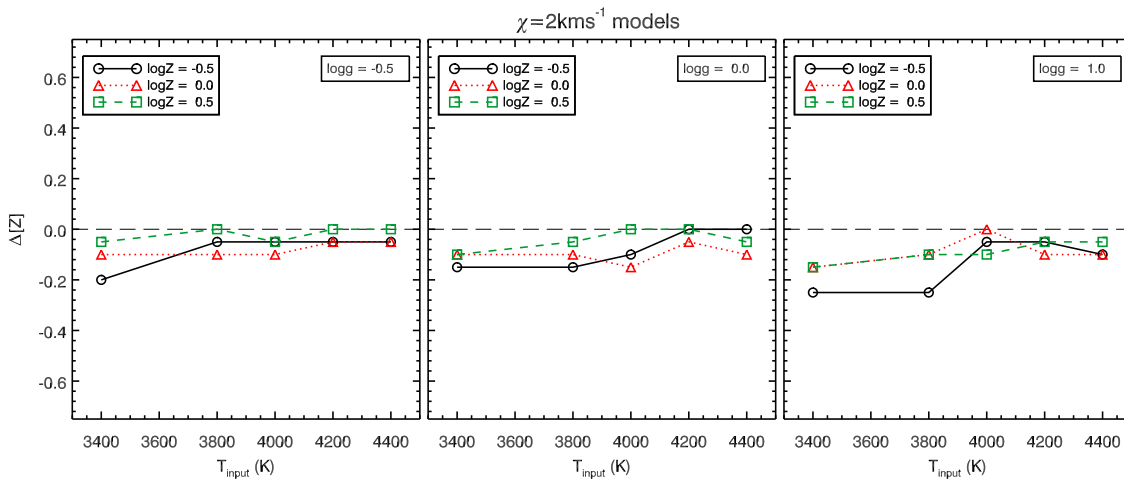
Fig. 12.— Influence of the Si I , Ti I and Fe I non-LTE effects on the DKF10 J-band χ^2 metallicity determination as a function of effective temperature. The numerical experiment is described in the text. Left: log g = −0.5, middle: log g = 0.0, right: log g = 1.0. Circles: [Z] = −0.5, triangles: [Z] = 0.0, squares: [Z] = 0.5

TABLE 1

TABLE 1

J-BAND Si I LINES

Elem.	λ Å	E_{low} [eV]	lower level	E_{up} [eV]	upper level	$\log gf$
(1)	(2)	(3)	(4)	(5)	(6)	(7)
Si I	11991.57	4.92	4s ^{3}P$^o_0$	5.95	4p ^{3}D$_1$	-0.109
	11984.20	4.93	4s ^{3}P$^o_1$	5.96	4p ^{3}D$_2$	0.239
	12103.54	4.93	4s ^{3}P$^o_1$	5.95	4p ^{3}D$_1$	-0.351
	12031.50	4.95	4s ^{3}P$^o_2$	5.98	4p ^{3}D$_3$	0.477

TABLE 2

NON-LTE ABUNDANCE CORRECTIONS FOR THE SI I LINES ($\xi = 2$ KMS^{-1})

T_{eff}	$log\ g$	[Z]	Δ_{SiI} 11984.20	Δ_{SiI} 11991.57	Δ_{SiI} 12031.50	Δ_{SiI} 12103.54
(1)	(2)	(3)	(4)	(5)	(6)	(7)
4400.	-0.50	0.50	-0.08	-0.12	-0.05	-0.13
4400.	-0.50	0.00	-0.13	-0.18	-0.09	-0.18
4400.	-0.50	-0.50	-0.19	-0.24	-0.14	-0.24
4400.	0.00	0.50	-0.07	-0.10	-0.05	-0.12
4400.	0.00	0.00	-0.13	-0.18	-0.09	-0.19
4400.	0.00	-0.50	-0.21	-0.26	-0.15	-0.26
4400.	1.00	0.50	-0.05	-0.08	-0.04	-0.09
4400.	1.00	0.00	-0.11	-0.16	-0.07	-0.17
4400.	1.00	-0.50	-0.20	-0.27	-0.15	-0.27
4200.	-0.50	0.50	-0.07	-0.10	-0.05	-0.12
4200.	-0.50	0.00	-0.12	-0.17	-0.09	-0.18
4200.	-0.50	-0.50	-0.20	-0.25	-0.15	-0.24
4200.	0.00	0.50	-0.06	-0.10	-0.04	-0.11
4200.	0.00	0.00	-0.12	-0.18	-0.09	-0.19
4200.	0.00	-0.50	-0.21	-0.27	-0.16	-0.27
4200.	1.00	0.50	-0.05	-0.08	-0.04	-0.10
4200.	1.00	0.00	-0.11	-0.16	-0.08	-0.17
4200.	1.00	-0.50	-0.21	-0.27	-0.15	-0.27
4000.	-0.50	0.50	-0.07	-0.11	-0.05	-0.13
4000.	-0.50	0.00	-0.13	-0.18	-0.09	-0.19
4000.	-0.50	-0.50	-0.21	-0.26	-0.15	-0.26
4000.	0.00	0.50	-0.07	-0.11	-0.05	-0.12
4000.	0.00	0.00	-0.13	-0.18	-0.09	-0.20
4000.	0.00	-0.50	-0.22	-0.28	-0.17	-0.28
4000.	1.00	0.50	-0.06	-0.09	-0.05	-0.11
4000.	1.00	0.00	-0.12	-0.17	-0.09	-0.18
4000.	1.00	-0.50	-0.22	-0.28	-0.17	-0.27
3800.	-0.50	0.50	-0.08	-0.12	-0.06	-0.14
3800.	-0.50	0.00	-0.15	-0.20	-0.10	-0.22
3800.	-0.50	-0.50	-0.23	-0.28	-0.18	-0.28
3800.	1.00	0.50	-0.08	-0.12	-0.06	-0.13
3800.	1.00	0.00	-0.15	-0.20	-0.11	-0.21
3800.	1.00	-0.50	-0.25	-0.30	-0.20	-0.27
3800.	0.00	0.50	-0.08	-0.12	-0.06	-0.14
3800.	0.00	0.00	-0.15	-0.21	-0.11	-0.23
3800.	0.00	-0.50	-0.25	-0.31	-0.19	-0.29
3400.	-0.50	0.50	-0.17	-0.24	-0.12	-0.26
3400.	-0.50	0.00	-0.30	-0.36	-0.22	-0.35
3400.	-0.50	-0.50	-0.39	-0.41	-0.33	-0.37
3400.	0.00	0.50	-0.19	-0.25	-0.13	-0.27
3400.	0.00	0.00	-0.33	-0.38	-0.25	-0.37
3400.	0.00	-0.50	-0.42	-0.43	-0.36	-0.37
3400.	1.00	0.50	-0.20	-0.24	-0.14	-0.25
3400.	1.00	0.00	-0.32	-0.35	-0.25	-0.31
3400.	1.00	-0.50	-0.38	-0.36	-0.33	-0.34

TABLE 3

EQUIVALENT WIDTHS [a] OF THE Si I LINES ($\xi = 2 \ \mathrm{km s}^{-1}$)

T_{eff}	$log\ g$	[Z]	$W_{\lambda,SiI}$ 11984 LTE	$W_{\lambda,SiI}$ 11984 NLTE	$W_{\lambda,SiI}$ 11991 LTE	$W_{\lambda,SiI}$ 11991 NLTE	$W_{\lambda,SiI}$ 12031 LTE	$W_{\lambda,SiI}$ 12031 NLTE	$W_{\lambda,SiI}$ 12103 LTE	$W_{\lambda,SiI}$ 12103 NLTE
(1)	(2)	(3)	(4)	(5)	(6)	(7)	(8)	(9)	(10)	(11)
4400	-0.50	0.00	381.3	402.9	350.5	373.6	403.6	422.6	330.6	351.7
4400	-0.50	0.50	426.2	444.8	392.5	412.3	452.3	468.7	372.0	390.0
4400	-0.50	-0.50	340.5	365.3	309.7	336.4	362.2	383.6	289.4	314.0
4400	0.00	0.00	369.4	393.8	337.4	363.3	393.3	414.8	317.3	340.8
4400	0.00	0.50	422.4	443.2	384.3	406.3	453.5	471.9	362.2	382.1
4400	0.00	-0.50	327.0	355.4	296.1	326.3	349.2	373.9	276.2	303.6
4400	1.00	0.00	348.9	378.3	311.6	342.3	379.0	405.0	289.9	317.2
4400	1.00	0.50	427.7	452.8	371.9	398.1	478.5	501.0	343.0	366.5
4400	1.00	-0.50	299.5	334.0	267.6	303.2	323.6	354.0	247.9	278.9
4200	-0.50	0.00	375.6	397.9	345.1	368.9	397.6	417.2	325.6	347.4
4200	-0.50	0.50	422.6	442.0	388.3	408.9	449.5	466.7	367.7	386.5
4200	-0.50	-0.50	335.9	361.7	306.0	333.5	356.9	379.4	286.3	311.5
4200	0.00	0.00	360.0	385.1	328.3	354.9	383.6	405.6	308.5	332.7
4200	0.00	0.50	415.4	437.3	376.2	399.2	448.0	467.4	353.9	374.8
4200	0.00	-0.50	317.8	347.0	287.7	318.7	339.1	364.6	268.3	296.3
4200	1.00	0.00	332.3	362.8	295.8	327.4	361.7	388.7	274.6	302.4
4200	1.00	0.50	412.6	439.8	356.2	384.3	464.4	488.7	327.1	352.2
4200	1.00	-0.50	283.9	318.9	253.3	288.9	306.7	337.8	234.2	264.8
4000	-0.50	0.00	363.6	387.9	330.2	355.8	389.3	410.7	309.7	333.1
4000	-0.50	0.50	423.3	445.8	377.2	400.7	463.6	483.6	351.9	373.4
4000	-0.50	-0.50	321.7	348.9	291.4	320.2	343.2	367.0	271.8	298.1
4000	0.00	0.00	349.1	376.5	312.4	341.0	378.6	402.8	290.7	316.7
4000	0.00	0.50	425.5	451.1	368.2	394.8	477.9	500.8	338.4	362.6
4000	0.00	-0.50	301.9	332.6	271.1	303.2	324.5	351.3	251.6	280.4
4000	1.00	0.00	329.4	362.9	282.5	316.5	370.3	400.3	257.1	286.5
4000	1.00	0.50	450.1	482.2	362.8	395.5	530.4	559.3	320.0	348.8
4000	1.00	-0.50	261.9	297.8	232.5	268.3	283.4	315.8	213.9	243.8
3800	-0.50	0.00	343.2	371.2	306.6	335.5	372.7	397.4	285.0	311.4
3800	-0.50	0.50	415.4	442.5	357.7	385.6	468.0	492.0	327.6	353.1
3800	-0.50	-0.50	299.0	328.6	268.5	299.2	321.0	347.0	248.9	276.7
3800	0.00	0.00	329.2	360.8	288.2	320.6	363.7	391.7	265.1	294.2
3800	0.00	0.50	420.6	451.2	349.9	381.4	485.2	512.3	314.1	342.6
3800	0.00	-0.50	278.8	311.8	247.5	281.1	302.1	331.4	227.9	257.5
3800	1.00	0.00	293.3	330.8	250.1	287.0	330.5	364.8	226.5	257.4
3800	1.00	0.50	402.1	438.6	323.4	360.0	474.3	506.9	284.4	316.3
3800	1.00	-0.50	238.9	276.1	207.7	243.3	262.6	297.3	188.4	216.8
3400	-0.50	0.00	260.8	298.9	228.6	265.9	286.3	319.1	209.5	243.1
3400	-0.50	0.50	324.6	360.8	275.8	311.9	367.2	398.2	249.6	283.3
3400	-0.50	-0.50	222.8	260.7	195.6	231.8	242.2	276.5	178.1	209.4
3400	0.00	0.00	240.6	281.6	206.7	245.8	267.9	303.8	187.0	221.2
3400	0.00	0.50	311.2	351.0	257.8	296.8	358.5	392.4	229.6	265.1
3400	0.00	-0.50	200.1	239.5	172.9	209.4	219.9	256.3	155.6	185.6
3400	1.00	0.00	204.8	245.3	167.4	203.2	236.2	273.4	146.6	174.9
3400	1.00	0.50	285.1	328.7	224.1	264.1	340.0	378.3	192.2	225.9
3400	1.00	-0.50	160.5	194.2	133.2	161.9	181.3	214.4	116.5	137.8

[a]equivalent widths W_{λ} are given in mÅ